PIV MEASUREMENT OF INJECTION PRESSURE INFLUENCE ON GAS ENTRAINMENT IN GDI-ENGINES

B. Prosperi[1,2], J. Hélie[2] and R. Bazile[1]

[1] Institut de Mécanique des Fluides de Toulouse, 31400 Toulouse, France. prosperi@imft.fr

[2] SIEMENS VDO Automotive, BP1149,1 av. Paul Ourliac, 31036 Toulouse cedex 1, France

ABSTRACT : The gas entrainment induced by a hollow-cone spray under various injection conditions is studied experimentally in order to evaluate the effects on mixture formation. Particle Image Velocimetry with Fluorescent tracers (F-PIV has been applied to allow measurements in the close vicinity of the spray-edge. Next, the obtained data (instantaneous velocity fields) have been processed in a specific way. In the "quasi-steady" region of the air-flow surrounding the spray, the injection pressure - and back pressure effects on the mass-flow rate of entrained gas can be predicted by a semi-empirical model that takes the injection parameters into account.

Keywords: GDI, piezo-electric injector, spray, Fluorescent PIV, injection pressure, gas entrainment

1. INTRODUCTION

To achieve fuel economy and to reduce pollutant emissions, a new generation of injectors has allowed to implement injection-strategies like lean-stratified combustion modes [1][2]. Based on stability and reliability criteria for the mixture formation, the "spray-guided" direct injection strategy has been chosen to optimize the combustion process. In a recent study, the benefits of Gasoline Direct Injection (GDI) with piezo-injectors has been shown by Siemens VDO Automotive [3]. These results are used in the present study. The main advantages of these injectors are their wide operating range and their highly reproducible injection behaviour. In a previous article [4], the influence of air-density on gas entrainment was studied under constant injection pressure. The present work deals with the influence of injection pressure on air entrainment in case of hollow-cone dense sprays (figure 1). The aim of the present work is to establish a link between mixture formation [5] and injection-conditions.

Rottenkolber et al. [6] have proposed an adaptation of the Particles Image Velocimetry using Laser-Induced Fluorescence (FPIV). This technique is used in the present study to measure air entrainment in dense two-phase air-flows.

Under realistic engine conditions, this method allows the measurement of the gas-velocity flow-field all around and very close to the spray edge. Moreover, when low-pressure injections are performed under atmospheric conditions, this method allows monitoring the gas velocity flow field inside the spray. A typical case is given as an illustration.

From the measurements performed under various conditions, the axial evolution of the air-entrained cumulative mass-flow rate is computed. Next, these results are compared with those obtained with an integral model [7] developed for an axi-symmetrical full-cone spray. Although this model shows good correspondence for the global flow-rate over the Z-axis with experimental results over the region of interest [8], the model does not correctly predict the local air velocity in a direction perpendicular to that of the surface of the cone. Whenever, a basic axial-evolution of the air-entrained velocity is proposed and fitted with a reference case. The injection global parameters dependence of the integral-model is used in combination with the empirical fit for the air-entrained velocity to enable a semi-empirical model to predict the effects under various injection conditions.

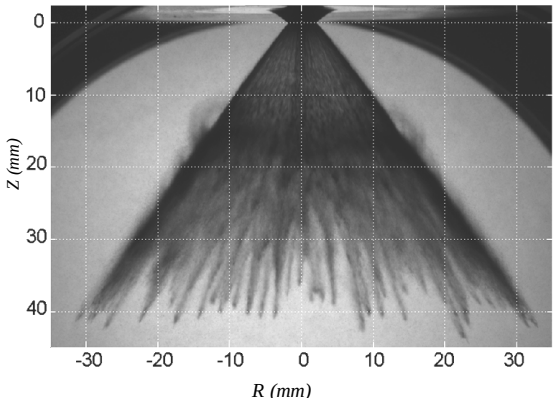

Figure 1: Gasoline injection spray.

2. EXPERIMENTAL APPARATUS

2.1 Injection test bench and spray characteristics

GDI automotive fuel system is used to pressurize gasoline up to 200 bars. The gasoline direct injector is an outward-opening piezoelectric driven one generating a 80° conical liquid sheet due to its annular shaped orifice (4.2 mm diameter). The atomization induced by this kind of injector produces very fine droplets that have been characterized under various injection pressures with Malvern Spraytech granulometer. As the spray is dense, measurements could be performed between 30 mm and 75 mm far from the nozzle under various injection pressures in atmospheric condition. As integrated measurements along laser path, results for droplet mean diameter should be taken with care and will be taken as rough estimations in the present study (Table 1). Finer PDA measurements [9] are on course to characterize precisely the droplet-size poly-dispersion distribution.

Concerning the stability-increase of the injection test bench, a low-pressure (LP) filling-pump at 5 bars combined with a mechanical pressure-regulator have been mounted backward the three-pistons high-pressure (HP) hydraulic pump that allows to pressurize the liquid. At full load when discharge losses become important, the LP pump allows to feed sufficiently the HP pump with liquid whereas at partial load, overpressures are avoided thanks to the regulator. Passing through a thermal exchanger implemented upward the fuel tank, the liquid is kept at a constant temperature of 20°. Let notice that a non evaporating fluid (Isane) is used in the present study, with properties close to gasoline.

Mean liquid mass-flow rate characterization on the updated setup has been performed under various injection pressures (P_{inj}) with an industrial measurement device (EMI2). Those measurements allow computing the discharge coefficient of the injector using needle-lift assumption so that the mean liquid velocity at injector's outlet (V_{inj}) should be estimated (Table 1).

Table 1: Injection pressure effects on PZ spray characteristics at nominal needle lift of 26 µm.

P_{inj} (bars)	50	100	150	200
d_p (µm)	15	12	10	9
m_l (g/s)	15	22	28	30
V_{inj} (m/s)	90	140	170	180

Both droplet size and mean liquid mass-flow rate under various injection conditions are used for the analysis of the gas flow motion induced by the spray as well as for the air entrainment model.

2.2 FPIV configuration

Injections are performed in a vessel equipped with optical accesses, the maximum relative-pressure inside being 12 bars. Figure 2 illustrates the experimental set-up for air entrainment measurement by F-PIV.

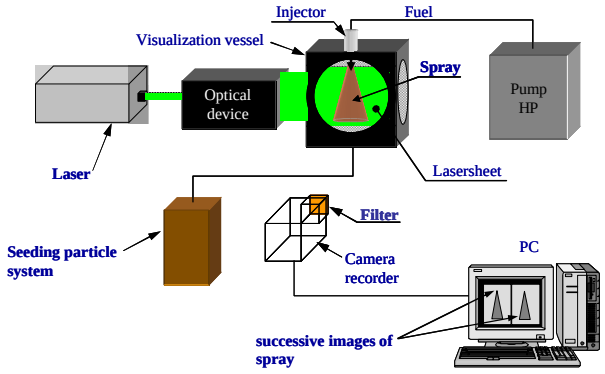

Figure 2: Experimental set-up for spray investigations

As our interest is to measure air entrainment induced by a spray using PIV technique, we have to keep in mind that video-sensor can be damaged while a dense liquid-area is illuminated. Thus we use here a FPIV technique in order to detect the tracers of the continuous phase at a shifted wavelength. On the one hand, the tracers must be small enough to follow the air motion around the spray. On the other hand, their fluorescent emissions must be strong enough to be detected by the camera. To fulfil these two conditions, a dye droplets generator has been designed to deliver seeding particles being sensitive with surrounding gas, i.e Stokes number inferior to unity. The tracers arising out of a propylene-carbonate (PC) solution saturated with dichloromethane (DCM) have interesting properties as their fluorescence emission wavelength vary between 615 and 666 nm and is maximum at 639nm [6]. A spectra-Physics Nd-Yag bi-pulse laser is used to excite the dyes ($\lambda_{excitation}$ =532 nm). An optical red-filter (OG590) is placed in front of the camera to reject the strong elastic-diffusion of the laser sheet by the spray. In spite of the 2/2 pixels hard binning, reducing the resolution of the camera to 520 x 688 but virtually increasing the sensor sensibility, the gray levels of the fluorescence signal remain low, in the range [50;300].

The synchronization of laser-pulses, video recorder gates and injection command is performed by several PC cards and dedicated software. The air velocity-range depending both on the injection conditions and on the size of observed region, the delay between two laser-pulses is tuned as a function of the setup configuration. As a result, this delay varies between 10 and 25 microseconds, respectively for high air-velocity monitoring (15 m/s) with high image resolution (30 µm/ pixel) and for low air-velocity monitoring (5 m/s) with low image-resolution (60 µm/ pixel).

3. RESULTS AND DISCUSSION

3.1 Gas entrainment calculation method

Traditional PIV algorithm using iterative cell shifting and deformation [10] is applied on the overall two-phase flow field. As liquid droplets can be mistaken with gas tracers, some vectors inside the spray can be spurious. A dedicated F-PIV algorithm based on the normalized median-filter [11] has been developed and leads to well filtered instantaneous flow fields.

The phenomenon being repetitive [4], the mean velocity-fields of entrained-air have been calculated by averaging 50 instantaneous FPIV fields. The continuity equation as well as the statistical convergence has been successfully verified for the gaseous phase.

As a means of evaluating the liquid/gas mixing process, the direct gas-entrainment measurement method is performed. The control surface used for the calculations is located close to the spray-edge (2 mm). The mass flux of entrained gas along the control surface between axial locations z1 and z2 is given by:

$$\dot{m}_e = \int_{z_1}^{z_2} \rho \bar{U}_{\perp} 2\pi r \frac{dz}{\cos(\theta/2)} \qquad (1)$$

Where $U_{\perp}$ is the mean velocity component defined perpendicularly to the conical surface at a distance of 2 mm from the spray-edge (cone angle ($\theta/2$)).

3.2 FPIV measurement analysis

REFERENCE CASE

The mean-velocity field (Figure. 3) obtained at 9 bars ambient back pressure (P_c) and 200 bars injection pressure is representative for high-pressure gasoline direct injection application which requires injection pressures higher than 100 bars and back pressure higher than 6 bars as injection starts late in the compression cycle. A quantitative study around this operational point has been performed and is reported in the following sections.

In the vicinity of the spray-edge, very close to the injector's outlet, external air is sucked directly toward the liquid sheet. Gas-velocity magnitude increases with axial distance from nozzle tip, reaching 9 m/s at Z = 10 mm, and is time independent. This area is defined as the "quasi-steady" (QS) entrainment zone contrary to the unsteady recirculation zone that develops at the spray front. A preliminary test has allowed verifying the "quasi-steady" assumption over the observed region defined along the spray axis from the nozzle up to the vortex zone.

By the means of plotting the frozen streamlines around the spray, one can observe two major vortex rings forming from both part of the liquid sheet. These mechanisms allow bringing far external air into the spray.

In typical GDI application, conditions are too constraining to plenty observe the phenomena. However, as injection pressure decreases, the liquid sheet velocity decreases and the atomisation process becomes less efficient. As a consequence and for low needle lift, the spray is sufficiently diluted so that, for atmospheric conditions, imaging of the tracers inside the spray remains good enough to validate PIV calculations.

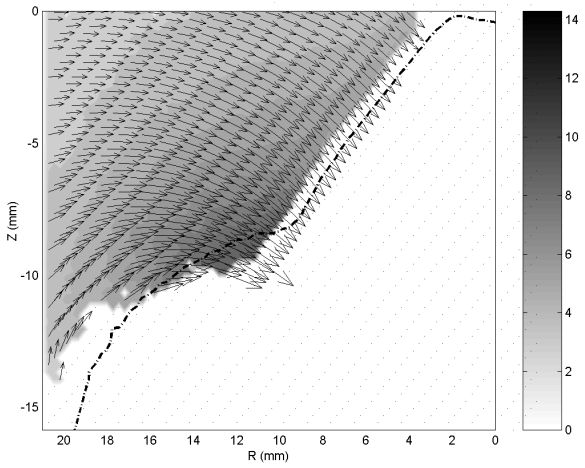

Figure 3: Mean velocity field of gas entrained by the spray 1.00 ms after start of injection. P_{inj} = 200 bars and P_c = 9 bars. Velocity magnitude (coloured surface) and gas / liquid mean interface (dash dot line).

LOW INJECTION PRESSURE CASE

The analysis of a downgrade case being of great help in the understanding of the mixing preparation, the temporal evolution of the gas flow motion is illustrated figure 4 and is described here after.

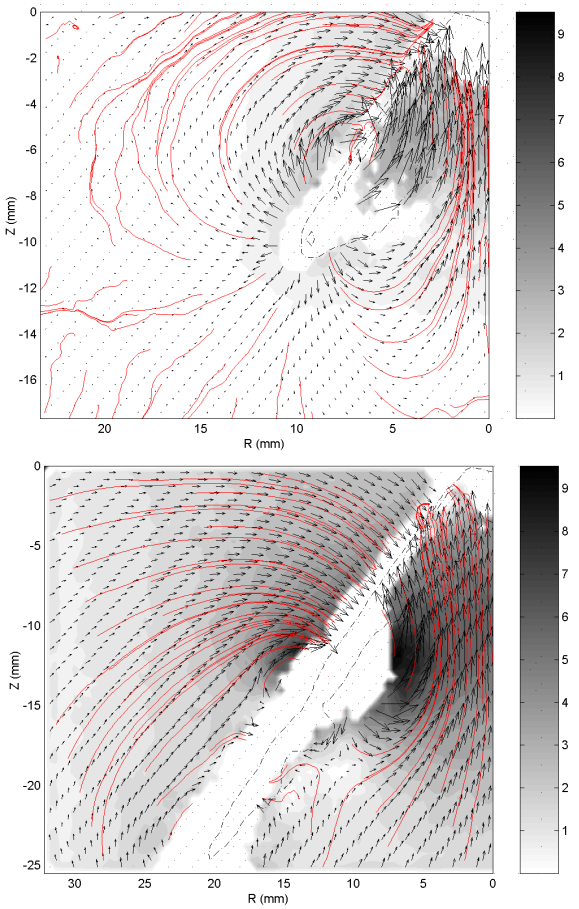

Figure 4: Gas velocity flow field obtained at 50 bars injection pressure and atmospheric back pressure at 0.30 and 1.00 ms after start of injection. Velocity magnitude (coloured surface) and frozen stream lines (red lines).

At the early stage of the spray formation (0.30 ms after start of injection (asoi)), the liquid introduction induces the starting motion of the surrounding air. External and internal vortex rings develops simultaneously from both part of the liquid sheet in a different way, as the frozen streamlines of the gas flow indicates. Whereas externally, the gas is circulating roundly from the spray front to the QS entrainment zone, internally, gas seems to circulate from the spray front to the nozzle. Concerning the external circulation, the centre of the vortex can be evaluated at the axial position Z ≈ 6 mm whereas the axial liquid penetration is close to 11 mm.

Later on (1.00 ms asoi), the QS entrainment zone has established itself, over a distance of 13 mm approximately, whereas the internal gas-entrainment is still different. As can be observed at the axial location Z= 16 mm on figure

4.b, a segregation of the liquid occurs. The main part of the liquid goes straight whereas the secondary part accumulates around the circulation, leading to two distinct parts of the spray. Due to the specific operating conditions of this case (P_{inj} = 50 bars, P_c = 1 bars), most of the droplets are weakly responsive with air, their Stokes number being superior to unity, and only very few droplets, whose Stokes numbers are smaller than unity, are responsive and can be caught by the circulation. Whether increasing the ambient density or decreasing the droplets size, most of the droplets becomes responsive with air motion so that the liquid stratified around the vortex rings to produce a compact spray.

3.3 Injection conditions effect on gas entrainment

In order to be representative with real engine conditions, CF4 gas, three time denser than air, is used to simulate densities higher than 3.6 kg/m3 (i.e. 3 bars air). As an example, CF4 gas is pressurized at 3 bars in order to study back pressure effect at 9 bars air equivalent (i.e 10.8 kg/m^3).

As can be seen on figure 3, gas velocities can be measured very close to the spray edge until the vortex zone. The effects of injection conditions are evaluated thanks to the axial evolution of the entrained-gas cumulative mass-flow rate monitored through a control line defined at 2 mm from the spray edge (40°) at the observation timing of 1.00 ms after start of injection.

BACK PRESSURE EFFECT

Entrained-air cumulative mass-flow rate has been measured for various ambient back pressures (from 1 to 15 bars). In order to avoid misunderstanding, the ambient density in the chamber will be considered instead of the air-equivalent back pressure.

Air-entrainment rate increases quickly along axial penetration whatever the gas density in the chamber. As can be seen (figure 5), the denser the environment is, the more the air-entrained mass-flow rate is. It is difficult to objectively compare the global air-entrainment efficiency as the length of the QS entrainment region as well as the cumulative mass-flow rate depends on the ambient density. As an example, the cumulative gas mass-flow rate is multiplied by 12 at a fixed axial location between the extreme cases whose density ratio is equal to 15, whereas the length ratio of the QS region is approximately divided by 3. Nevertheless, the interaction between the surrounding gas and the fuel droplets are enhanced when ambient density increases without apparent effect of saturation.

INJECTION PRESSURE EFFECT

The axial evolution of the entrained-gas cumulative mass-flow rate for various injection pressures is presented in figure 6. The results indicate that the more injection pressure is, the better the air-entrainment process is. Indeed, when injection pressure increases, the atomisation is enhanced and, finally, very small droplets are produced. As a consequence, the exchange surface between the gas and the liquid is increased so that the interaction between the surrounding gas and the fuel droplets are enhanced.

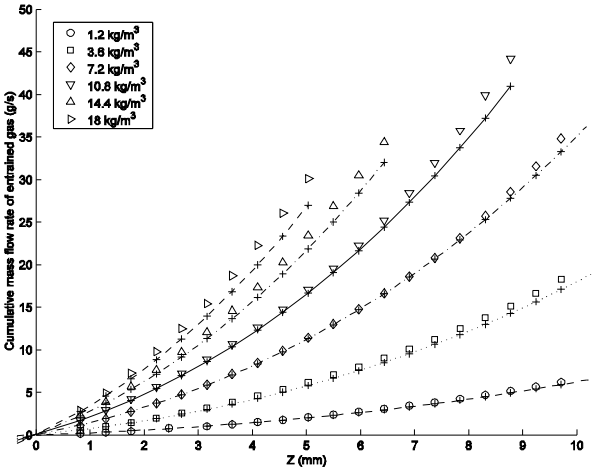

Figure 5: Axial evolution of the entrained gas cumulative mass-flow rate for various ambient densities at 1 ms asoi. P_{inj} = 200 bars.
Symbols: FPIV measurement, lines: semi-empirical model.

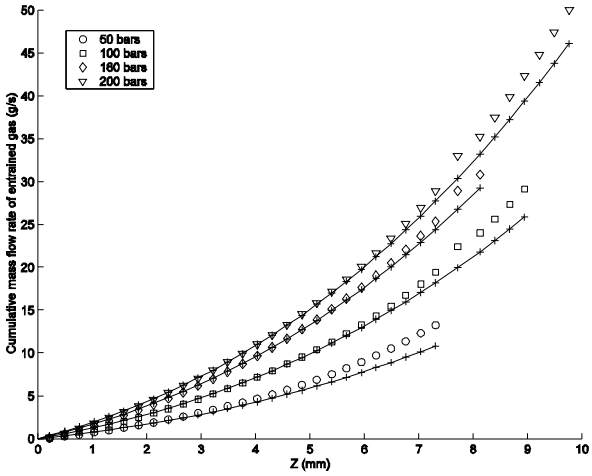

Figure 6: Axial evolution of the entrained gas cumulative mass-flow rate for various injection pressures at 1 ms asoi for P_c = 9 bars (ρ_{air} = 10.8 kg/m^3).
Symbols: FPIV measurement, lines: semi-empirical model.

3.4 Comparison with an integral model

The experimental results are compared with a 1D-model proposed by Cossali's [7]. This model, developed for non-evaporating full cone steady spray injected into quiescent gas, relies on continuity equation and momentum exchanges between liquid and gaseous phases. In the gas-entrainment zone, the liquid velocity of the dense spray is so high that the relative slip-velocity between gas and liquid is close to one. However, droplets submitted to aerodynamic drag effect decelerate and transfer momentum to ambient gas. In this "transfer area", momentum

exchange between phases increases progressively as axial distance increases before decreasing in the "vortex area", far from the atomization origin. The transfer area can be decomposed into two distinct zones: "near" and "far" fields. In the near field, jet is so dense that gas-entrained cumulative mass-flow rate is supposed to follow a 3/2 power-law axial evolution whereas in the "far" field, a linear dependence is found like in dilute particle laden jets. As a consequence, the air-entrainment velocity axial evolution is supposed, first, to evolve in square root of z and, next, to tend to a constant value at infinity:

$$\text{For } z \to 0, \quad U_{\perp} = \beta_{near}.z^{1/2}.\left(\frac{3}{2} - \frac{1}{2} z_0 z^{-1}\right) \qquad (2)$$

$$\text{For } z \to \infty, \quad U_{\perp} = \beta_{far} \qquad (3)$$

As can be seen in figure 7, the entrained-gas velocity increases as a function of the axial distance in a way quite different from the one predicted by the integral model. Due to the downstream and upstream experimental boundary conditions, neither the rapid increase for $U_{\perp}$, in the near field, nor the asymptotic value for $U_{\perp}$, in the far field, can be observed. In the near field, the gas flow is probably influenced by the upper wall whereas, in the far field, the gas flow is influenced by the unsteady effect of the vortex ring. The model is not adapted to the air-entrainment induced by a GDI spray as the asymptotic behaviour could not be recovered with the actual setup.

Despite the unsuitable axial evolution air-entrained velocity, the injection parameter's dependence K proposed by the integral model shows good correspondence with ambient density-, droplet size- and liquid mass-flow rate variations. Thus, the parameter K for injection conditions variations has been tested in combination with a 1st order axial evolution for $U_{\perp}$ (eq. 4) in order to predict the axial evolution of the cumulative air-entrained mass-flow rate.

$$U_{\perp(z)} = c_0 + c_1.z + O.(z^2) \qquad (4)$$

c_0 and c_1 are fitted accordingly with the reference case at 200 bars injection pressure and 9 bars back pressure at a distance *dec* from spray edge.

Although a value slightly higher than 5/6 for the power-law dependence of ambient density is needed in order to fit satisfyingly with ambient density effect (figure 5), the -2/3 and 5/6 power-law dependence of the mean droplets diameter and the liquid mass-flow rate, respectively, gives convincing results (figure 6).

The use of a linear axial evolution for $U_{\perp}$ leads to a semi-empirical expression for the air entrained cumulative mass-flow rate in the form:

$$\dot{m}_e = \int_0^z 2\pi.\rho_g.U_{\perp(z^*)}.(m.z^* + n).\frac{dz^*}{\cos\left(\frac{\theta}{2}\right)} \qquad (5)$$

$$U_{\perp} = K.\left(\frac{\rho_{g\_ref}}{\rho_g}\right).(c_{0\_ref} + c_{1\_ref} z) \qquad (6)$$

$$K = \left(\frac{\rho_g}{\rho_{g\_ref}}\right)^{5/6}.\left(\frac{\dot{m}_l}{\dot{m}_{l\_ref}}\right)^{5/6}.\left(\frac{D_p}{D_{p\_ref}}\right)^{-2/3} \qquad (7)$$

$$m = -\tan(\theta/2) \qquad (8)$$

$$n = \frac{D_{injector}}{2} + \frac{dec}{\cos(\theta/2)} \qquad (9)$$

Where *m* and *n* take into account the conical aspect and *K* is the parameter's dependence coefficient from the integral model.

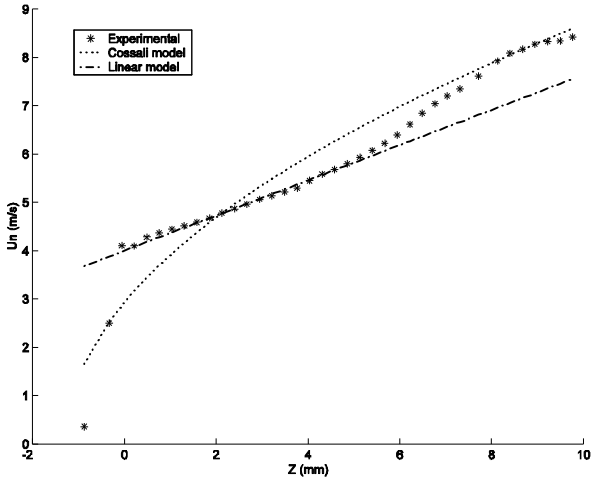

Figure 7: Axial evolution of normal velocity of entrained gas at 2 mm from spray edge (P_{inj} = 200 bars, P_c = 9 bars).
Symbol: FPIV measurement, dotted line: integral model (β_{near}=48) , dashed line: linear model (c_{0_ref} = 4; c_{1_ref} = 364).

The validity of the present approach is relative to the QS entrainment-zone in the injector's "near" field, i.e. up to the transition zone between two distinct regions where the liquid droplet concentration is "extremely"- or "less" dense. Indeed, as can be seen on the reference case (figure 7), the axial evolution of the velocity-gradient implies that momentum transfer between gas and liquid remains at a constant level up to an axial distance of 5 mm. Then, the velocity gradient reaches a higher value before decreasing in the vortex zone (located at Z = 8 mm). As a consequence, a "far" field model would be suitable to fit the experimental results on the overall "quasi-steady" region.

4 CONCLUSIONS

This paper presents data and analysis related to gas-entrainment into a high-pressure GDI spray. The reliability of the injection test bench allows studying the spray produced by a piezoelectric high-pressure injector.

The hollow-cone spray, induced by the annular shaped orifice, is described through the characterization of the liquid exiting the nozzle under various injection pressures.

The PIV on fluorescent tracers (F-PIV) is used to measure air-velocity in the close vicinity of the spray-edge. The main advantage of this technique is to avoid strong constraints concerning the powerful laser beam reflection induced by the crossway between the laser sheet and high liquid concentration area. Despite the use of fluorescent tracers, the spurious contribution of the liquid phase remains still visible on the F-PIV images. Following the approach proposed by [11], a dedicated post-treatment of the instantaneous gas-velocity flow field has been applied to eliminate persistent wrong vectors.

Thanks to this method and its associated post-treatment, the gas motion induced by a GDI spray can be studied by an ensemble-averaged method. As an example, a low-pressure injection case in atmospheric conditions is described and brings complementary information on mixture formation. The difference between the internal and external air entrainment is put on light.

A direct measurement method for gas-entrainment has been applied in the "quasi-steady" gas-flow region of a GDI spray to compute the cumulative gas-entrained mass-flow rate axial evolution. Important gas density effects have been pointed out. The denser the environment is, the more the surrounding gas will interact with the fuel droplets. An integral model developed for Diesel full cone spray (Cossali, 2001) has been investigated to better understand the gas/liquid momentum exchange. Whereas the local gas entrainment rate could not be well estimated, the global dependence of injection conditions variations can be predicted by the model. A semi-empirical model using the integral model dependence with the injection parameters and an empirical fit for the air-entrained velocity axial evolution is then proposed. The comparison between the experimental- and the semi-empirical model results gives satisfying results. The more the injection pressure is, the more the liquid-mass-flow rate is and the smaller the droplets are. Interactions between gas and liquid clearly depend on injection conditions and the mass-flow rate of entrained gas in the "near field" is found to scale like $K.(\varphi.z+\kappa.z^2+\lambda.z^3)$.

Further works are still in progress to take advantage of the semi-empirical entrainment model for 3D CFD simulation and to understand the air/fuel mixing process in GDI sprays.

5 NOMENCLATURE

asoi	after start of injection [s]
d	diameter [m]
dec	distance to spray edge [m]
m	mass-flow rate [kg/s]
P	pressure [bar]
r	radial distance [m]
V	Velocity [m/s]
z	axial distance [m]
λ	wavelength [m]
ρ	density [kg/m^3]
θ	cone angle

Subscript

c	chamber
e	entrained-gas
g	quiescent gas
l	liquid
p	droplet
inj	injection
ref	reference
s	spray
0	initial
$\perp$	perpendicular

6. REFERENCES

1. Zhao, F., Lai, M.-C., Harrington, D. L., Automotive spark-ignited direct-injection gasoline engines, Progress in Energy and Combustion Sciences, n°25, 1999.
2. Schwarz, C., Schunemann, E., Durst, B., Fischer, J., Witt, A., Potential of the Spray-Guided BMW DI Combustion System, SAE 2006-01-1265, 2006.
3. Achleitner, E., Berger, S., Frenfel, H., Klepatsch, M. and Warneck, V., Benzin-Direkteinspritzung auf Piezo-Basis, MTZ 5/2004 Jahrgang 65, 2004.
4. Delay G, Analyse des écoulements transitoires dans les systèmes d'injection directe d'essence, effets sur l'entrainement d'air instationnaire du spray, PhD Thesis, INP Toulouse, France, 2005.
5. Ghosh S., Hunt J. C. R. , Induced air velocity within droplet driven sprays. Proc. R. Soc. Lond. A 444, 1994.
6. Rottenkolber G. and al. Spray analysis of a gasoline direct injector by means of two-phase PIV. Experiments in Fluids, 2002.
7. Cossali G. E., An integral model for gas entrainment into full cone sprays. J. Fluid Mech., Vol. 439 : 353-366, 2001.
8. Prosperi B., Delay G., Bazile R., Helie J., Nuglish H.J., FPIV study of gas entrainment by a hollow cone spray submitted to variable density, Exp. Fluids, DOI 10.1007/s00348-007-0304-4.
9. Wigley, G., Pitcher, G., PDA Analysis of a polydisperse GDI fuel spray with dropsize class discrimination. ILASS Europe, Zürich, Suisse, 2001.
10. Lecordier, B., Trinité, M, Advenced PIV algorithms with image distorsion validation and comparison using synthetic images of turbulent flow, Proceedings of EUROPIV2 workshop, Zaragova, 2003.
11. Westerweel J. and Scarano F., Universal outlier detection for PIV data. Experiments in Fluids, 2005.

Corresponding author:

Brice PROSPERI

IMFT / SIEMENS VDO Automotive

E-mail: prosperi@imft.fr